A laboratory study of spray generation in high winds

IOP Conf. Series: Earth and Environmental Science **35** (2016) 012008 doi:10.1088/1755-1315/35/1/012008

A laboratory study of spray generation in high winds

D G Ortiz-Suslow, B K Haus, S Mehta and N J M Laxague

4600 Rickenbacker Causeway, Department of Ocean Sciences, Miami, FL 33149 USA

E-mail: dortiz-suslow@rsmas.miami.edu

E-mail: bhaus@rsmas.miami.edu

Abstract. Characterizing the vertical distribution of large spray particles (i.e., spume) in high wind conditions is necessary for better understanding of the development of the atmospheric boundary layer in extreme conditions. To this end a laboratory experiment was designed to observe the droplet concentration in the air above actively breaking waves. The experiments were carried out in hurricane force conditions (U_{10} equivalent wind speed of 36 to 54 m/s) and using both fresh water and salt water. While small differences between fresh and salt water were observed in profiles of radius-integrated spray volume fraction, the profiles tend to converge as the wind forcing increases. This supports the assumption that the physical mechanism for spume production is not sensitive to salinity and its corresponding link to the bubble size distribution.

1. Introduction

A respectable body of knowledge has been amassed regarding the open ocean exchange of momentum, energy, and gas across the ocean-atmosphere interface in light and moderate winds. However, information regarding these fluxes in high wind conditions remains limited. The atmospheric boundary layer becomes spray-ridden in wind speeds (referenced to a height of 10 m) above 30 m/s [1]. This has significant implications for modeling the balance between moist enthalpy input and wind energy dissipation at the air-sea interface and its impact on tropical storm development. It has been observed, in both laboratory [2] and field experiments [3, 4], that the creation of a defined spray layer coincides with the saturation of the atmospheric drag coefficient in the vicinity of 30 to 40 m/s. The fundamental mechanism that explains this remains elusive, but from a theoretical perspective it can be readily shown that the presence of spray in the bottom of the atmospheric boundary layer would alter the wind speed profile and subsequently the interfacial fluxes [5]. However, there is a dearth of direct knowledge regarding the effect that this increasing amount of entrained sea spray has on the air-sea flux of heat and momentum. Determining the relationship between sea spray and these transfer processes is critical for understanding the rate of intensification of tropical cyclones [6].

Particles with radii exceeding 25 µm are of particular interest as these have been shown to be the most significant to these processes [7, 8]. These spray droplets, also known as spume, are generated via wave breaking or wind shear tearing off the wave crests [9, 10]. Spume is generated in a range of sizes and it is expected that the presence of these large particles (50 µm–600 µm) will have an effect on the wind stress that is applied to the ocean surface. A number of theories exist that attempt to describe the role spray has on the transfer of momentum from the atmosphere to the ocean surface. Andreas [11] proposed that the falling droplets suppress the short wave development, which carry the majority of the wind stress. Also, while the wind forcing

increases with wind speed, the amount of stress carried by the particles also increases and this effectively decreases the momentum transfer coefficient. An alternative theory is proposed by Barenblatt *et al.* and Bye and Jenkins [12, 13], who suggest that a spray-infested layer develops that essentially masks the ocean surface from direct physical interaction with the atmosphere. Soloviev and Lukas [9] suggest that due to the high wind shear the spray and spume production stabilizes the ocean surface and small waves become height-limited as their crests are blown off.

The presence of entrained spume particles can also act as an important thermodynamic layer between the atmosphere and ocean and is expected to affect the air-sea enthalpy flux. Taking into account the three-dimensional transport of a size-dependent distribution of aerodynamic particles that thermally interact with the ambient, turbulent flow is a challenge. Therefore, microphysical models proposed by Andreas [14], and expanded by Andreas and Emanuel [15], Andreas [16], and Andreas *et al.* [17], attempt to explain these dynamics in terms of the relevant time scales for droplet suspension, temperature evolution, and change in particle radius. A natural reference height for these models is the significant wave height, H_s, where the spray is expected to be generated at this level, travel through the atmosphere, and fall back to the surface where it can be considered coalesced with the ocean [17]. Jeong *et al.* [18] suggest that this physical description may change in strongly forced waves, where there is the potential for spray to impinge on the downwind wave slopes.

The role that spray and spume play in the fluxes across the air-sea interface all rely on some fundamental knowledge regarding the rate of particle production and the vertical distribution in the boundary layer. Accomplishing this in extreme conditions in the field is an arduous, if not impossible, task and so models and laboratories remain the primary sources of meaningful insight into these processes [19]. Currently, few laboratory experiments describe the vertical distribution of spume particles in either fresh or salt water in the strong wind forcings relevant to extreme oceanic conditions.

The results of a laboratory experiment focused on obtaining direct observations of the vertical distribution of large spume particles in very high winds are presented here. A nonintrusive, optical method is used to image spray droplets at a range of heights above the mean water level (MWL) in U_{10} equivalent winds ranging from 36 to 54 m/s. The particles observed range in radii from 86 µm to 1386 µm and experimental trials were conducted in both fresh and salt water. It is well known that bubble production in salt and fresh water exhibits distinct differences in the size and number of bubbles produced. While this is likely to have a large impact on spray aerosol production through the bubble bursting mechanism, it is not known whether this will significantly impact spume production. Here we seek to determine if there are significant differences in spume production for salt and fresh water. This will be important for comparing datasets collected over water bodies with different salinities.

2. Data collection

The observations were made in the University of Miami Air-Sea Interaction Saltwater Tank (ASIST), which is a wind-wave-current flume with a 15 x 1 x 1 m acrylic test section (see figure 1). Spray observations were made 11.05 m downwind of the air inlet. Maximum sustained winds, as measured by a sonic anemometer 6.6 m downwind of the inlet, reached ∼54 m/s when referenced to 10 m. This scaling follows similar work in ASIST by Donelan *et al.* [2] and Haus *et al.* [20]. A reference water depth of 0.42 m was used for all of the experiments.

Spray droplets were imaged using a modified Dantec Dynamics PIV (particle image velocimetry) acquisition system, where the laser sheet was re-routed through a liquid light guide to a strobe equipped with a telecentric lens, which produces a columnar beam of light (i.e., essentially non-convergent) that enhances the image contrast as opposed to a standard diffuse light source. This technique is similar to the direct imaging technique described in Christensen and Thomasson [21] and has been shown to be a robust and relatively straightforward method for

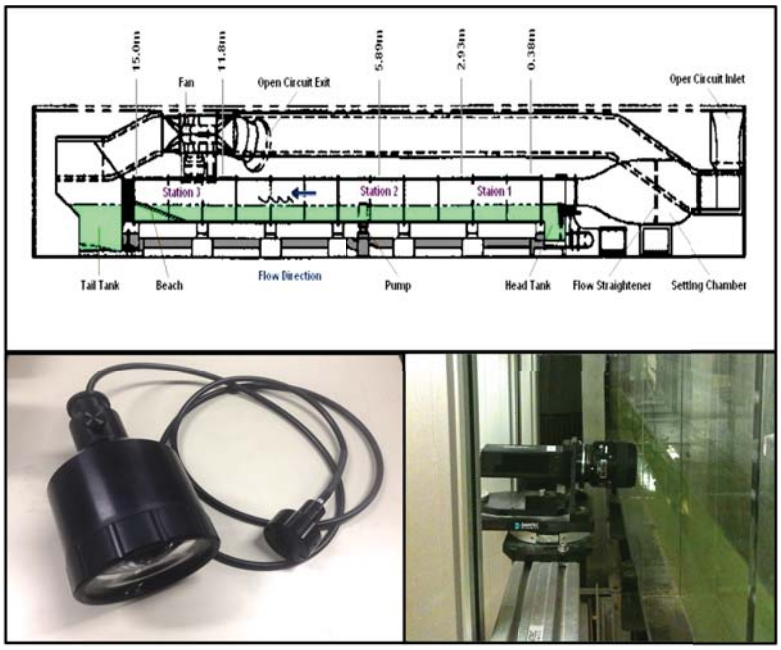

Figure 1. Clockwise from top: a schematic of the ASIST; the camera used for the data collection shown here on the vertical traverse that enabled multi-level imaging; the strobe and liquid light guide, which was mounted on another traverse (not shown) opposite the camera. The green tinge in the water is from a fluorescent dye, the observations presented here were done with clean, non-dyed water for both fresh and saline conditions.

quantifying particle statistics. This method differs from other optical techniques used in similar-style laboratory experiments [22], such as phase Doppler anemometry, which use convergent light sources to back-light particles and require more extensive cross-sectional area calibrations [23].

The camera used here (JAI CV-MSCL, 1.9 MP, 30 fps) was equipped with a medium telephoto lens (field of view 23.3°). This lens exhibits a magnification (pixels per meter) dependence on the depth of field; however, in practice this potential source of error is relatively small. Given that the focal plane was calibrated at 0.59 m from the lens (i.e., this is the focusing distance approximately at the center line of ASIST) and the depth of field of this lens is of order 3 mm, the potential magnification error in the particle sizing is around 1%. This source of error is much less than the uncertainties in the particle sizing algorithm used for this study, discussed further in section 3.

The collimated light beam was directed onto a diffusing screen (to reduce intensity) and the camera was oriented opposite the light source such that the optical axis of both strobe and camera were colinear. This camera-strobe system (including screen) was oriented perpendicular to the test region and mounted outside of the acrylic walls of ASIST. This meant that any spray droplets passing between light source and camera appeared as two-dimensional shadow projections (or silhouettes). The advantage of using this imaging method was that the images could be calibrated at a single focal plane [21], which was located in the middle of the ASIST control volume and oriented in a plane perpendicular to the along-tank direction. This experimental set-up enabled 42 µm per pixel resolution.

Five trials were conducted with wind speeds ranging in U_{10} equivalent magnitude from 36 to 54 m/s. For each trial, the tank was allowed 120 s to achieve steady state and then several image collections were acquired continuously, which generally took about 175 s to complete. For

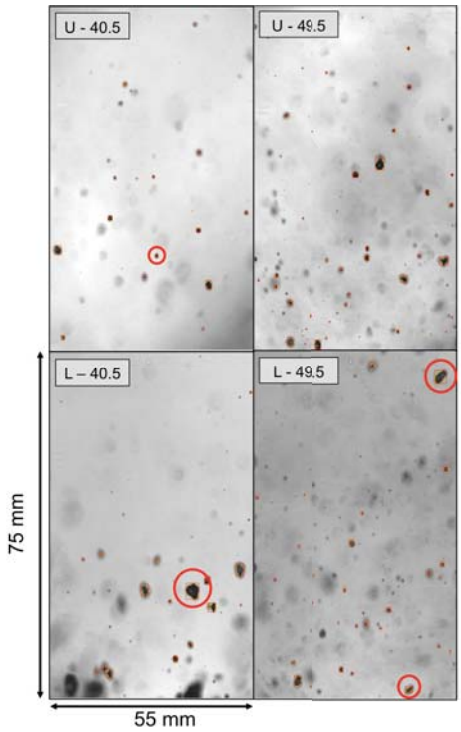

Figure 2. Sample images from the spray imaging data set. The U (L) refers to the upper (lower) level images and the number refers to the U_{10} equivalent wind speed. The red boxes and yellow circles represent particles identified and contoured by the automatic processing algorithm. Clockwise from upper left, the red-circled droplets have area equivalent radii of 92.5, 303.5, 181.5, and 396 µm.

each collection a total of 250 image pairs (i.e., 500 total frames) were acquired. The timing is precisely controlled by the Dantec software, and the frames within a pair were separated by 500 µm, with respective pairs sampled at 66.667 milliseconds (or 15 Hz). These five wind trials were repeated for both fresh and salt water. The salt water was 2 µM filtered sea water pumped in from a nearby tidal inlet, which can be considered a fully marine environment with no nearby fresh water sources.

In order to capture the vertical variability, each wind trial was sampled at different heights above the MWL. The salt water data were sampled at two reference heights, with the image frames centered at 95 mm (lower level) and 145 mm (upper level) above the mean surface. The fresh water data were sampled at three vertical levels, with frames centered at 95 mm, 145 mm, and 195 mm, respectively. Each individual experimental trial (i.e., water condition, a given wind speed, and reference level) was conducted independently with initial conditions in the tank being restored before another data set was collected. In total, this spray data set represents over 70,000 individual frames.

3. Data processing

The images were processed with a Dantec Dynamics shadow imaging software package using a two-step procedure. While image pairs were acquired, only one image per pair was used to compute the particle statistics. In the early stages of the image processing it was discovered that the sampling interval between pairs was too large to properly resolve the particle advection reliably across the entire data set, but single images were sufficient to determine droplet statistics. In the first step, each raw frame was balanced in order to correct for irregularities in the background light intensity of the imaged area. A collection of 250 frames was analyzed to determine the mean light sheet, then individual frames from this set of 250 were balanced according to this mean. Because this analysis was applied adaptively to each set independently, the overall light intensity reduction as the images became filled with droplets at the highest wind speeds was automatically taken into account. This helped enhance the image contrast across

the entire data set and normalize the images towards a standard gray level contrast between the background and the particles. A droplet identification algorithm was then applied to these now-balanced frames. The algorithm was trained on a single frame in order to determine baseline gray level contrast and particle edge gradients. The results of this training were then applied to the entire set of 250 images. This procedure was repeated independently for each respective collection of 250 frames (i.e, given a water state, wind speed, etc.).

This semi-automatic algorithm allowed this extensive data set to be processed far more expeditiously and consistently than if it had been manually analyzed. An attempt was made to quantify the success rate of this method and provide some confidence in its skill as a first step in post-processing quality control. For each 250-image collection, every 25th frame was visually inspected in order to ground truth the automatic detection algorithm. The automatic processing successfully identified (and sized) 75–90% of the droplets for all the data except those in lowest wind speed trial, which was only able to identify just above 60%. This discrepancy can be reasonably explained by low image contrast and variability in the light sheet that could not be adequately balanced in the processing. Also, a radius dependence was observed in the success rate, with the algorithm far more likely to miss the smaller particles (a few pixels across in diameter) as opposed to the larger drops (these were nearly always identified correctly). This was done for both experiments. The algorithm was observed to work significantly better with the later data set. This discrepancy in data quality could exist for various reasons due to variable image collection conditions that could not be rectified via the processing algorithm. The results presented in section 4 only include fresh water trials that were deemed acceptable given the results of the user-verifications.

4. Results

Spray concentration was observed to increase with wind speed and decrease with height above the surface. This was quantified following [24] as the number of particles per unit air volume per discrete radius interval,

$$n(r_i, z_j) = \frac{Count(r_i, z_j)}{a(z_j)Udtdr}, \tag{1}$$

where i and j are simply indices. The $Count(r_i, z_j)$ is the total number of particles for a particular vertical bin and radius class, $a(z_j)$ is the cross-sectional area of the vertical bin, U is the wind speed, dt and dr are the time interval and radius increment (here 50 µm), respectively. The along-tank and vertical extent of the total sampling volume was 55 mm and 75 mm, respectively, with a corresponding across-tank extent of 70 mm. This across-tank extent was determined in post-calibration as the operational depth of field. This was quantified using a standardized target with circles of known diameters between 1 and 2.5 mm. Investigations into the particle detection algorithm results revealed that the edge-detection method could not discriminate out-of-focus particles to the precision of the depth of field of the equipped lens (i.e., ± 1.5 mm). Thus the across-tank dimension used here can be considered the effective region sampled within each image by the particle detection method. By examining the grayscale gradient on the edge of out-of-focus standardized circles, this across-tank dimension (i.e., operational depth of field) was found to be largely size-independent. The vertical dimension used to estimate the air volume was 3 mm or the resolution of the profile.

The $n(r, z)$ for the highest (54 m/s) and lowest (36 m/s) wind conditions in both fresh and salt water (figure 3) provide a two-dimensional view of the droplet concentrations and show the filling of the laboratory air boundary layer with spume particles. For all particle sizes, the number concentration tends to decrease with height above the surface and increase with wind speed. The vertical gradients in number concentration for the smallest observed particles <200 µm tend to reduce with increasing wind speed, as in the z dependence becomes negligible.

Table 1. Percent of the $n(r, z)$ that was observed to be "empty" for fresh and salt water in all wind speed conditions considered in this study. Examples of the distributions are given in figure 3.

	Wind Speed			
Water Type	36 m/s	40.5 m/s	49.5 m/s	54 m/s
fresh	85.3	70.6	53.3	44.9
salt	84.5	65.5	37.0	32.4

However, this never occurs for the particle radii approaching 1 mm as their strong vertical gradients persist even during the strongest wind forcing. The height above the MWL here is scaled by the respective H_s,

$$H_s = 4\sqrt{m_0}, \tag{2}$$

where m_0 is the 0^{th} moment of the surface elevation variance spectrum derived from time series collected via an Ultrasonic Distance Meter (UDM), which was sampled at 10 Hz and located 5 m upwind of the imaging system used here.

In comparing fresh water to salt water, the distributions in figure 3 appear qualitatively similar, but some subtle differences exist, which warrant highlighting. The number concentrations are presented here as a two-dimensional particle density distribution that is a

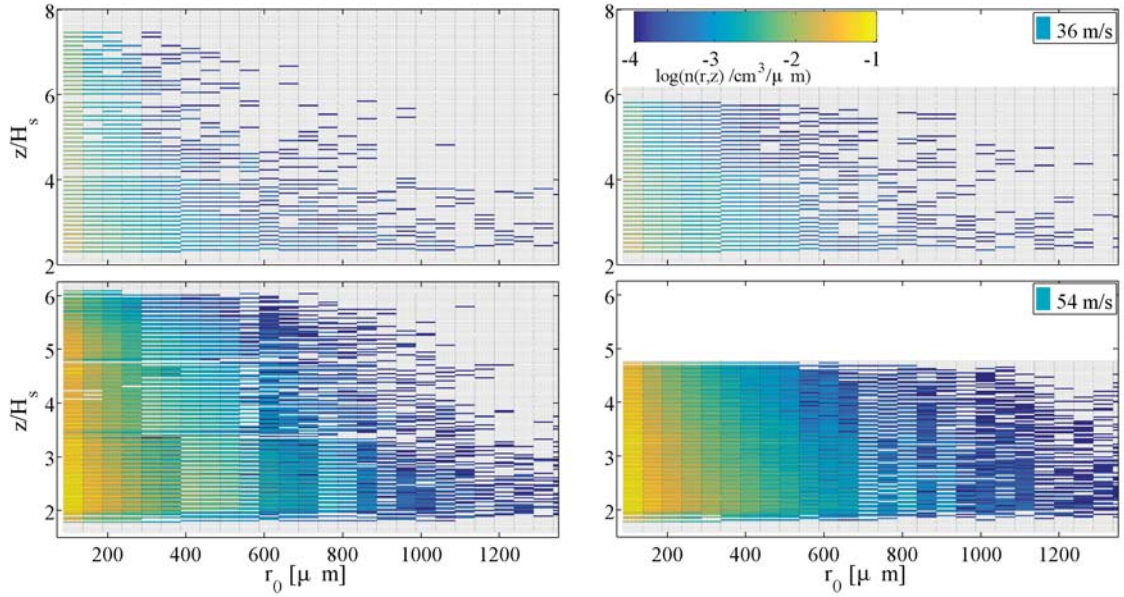

Figure 3. Two-dimensional distributions of number concentration as a function of height and observed particle radius for fresh (left column) and salt (right column) water. The lowest wind speed (upper row) and highest wind speed (lower row) trials are provided for comparison. Color refers to the log-scaled number of particles per unit air volume per radius class, the color scales are equivalent across the four panels. Grayed cells represent no particles counted, white regions represent unsampled physical space.

function of z/H_s and r (the latter is the observed radius). For fresh water, this distribution is concentrated in the small particle regime of the observed spectrum, while for saline conditions this distribution is far broader. This is evidenced by the relatively higher number concentrations observed in salt water opposed to fresh water out to an observed radius near 600 µm. This is seen at 36 m/s, but becomes more obvious in the 54 m/s wind trials (figure 3).

This may be quantified by the "emptiness" of the distribution. Given the discretization done in the averaging, there are portions of these arrays where no particles are actually counted for a given (z/H_s,r) coordinate (this information in terms of percentage for both water states is given in table 1). These percentages were only calculated over the shared vertical extent between the two data sets. There is a clear trend of decreasing emptiness with increasing wind speed, but this transition occurs faster in the saline water. From the distributions it is evident that this filling occurs most significantly in the larger particle regime. This may provide some evidence of the limiting effect of evaporation in the salt water, where particles can only lose a certain amount of volume during their aerial transport [24].

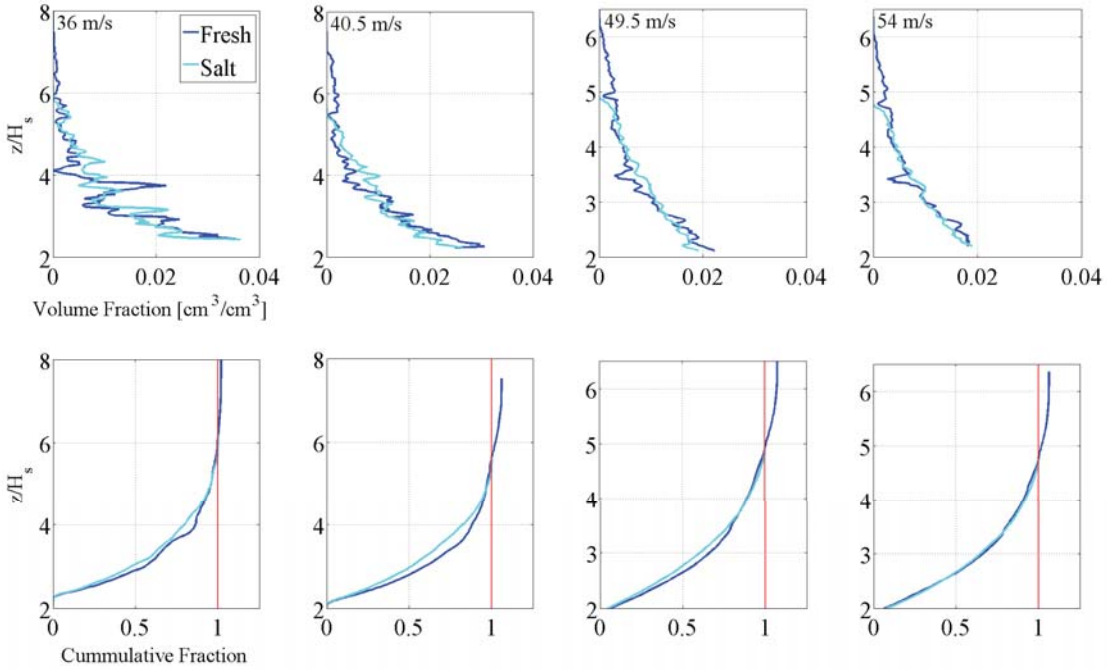

Figure 4. (Upper row) The total spray volume fraction profile for fresh and salt water across all wind speed conditions. (Lower row) Corresponding cumulative summation. Note, the fresh water was normalized up to the top of the salt water profile in order to make a fair comparison across data sets—this explains the >1 cumulation.

To highlight the vertical dependence, the radius-integrated $n(r, z)$ can be scaled into spray volume fraction profiles, as in the volume of spray observed in a vertical bin per total spray volume observed across the entire profile (figure 4). In order to reduce noise due to the discretization, these profiles have been smoothed with a running median filter two vertical bins wide. The profiles for fresh and salt water are generally similar in shape, but consistently in fresh water more spray volume is lost vertically than is observed to occur in salt water. This can also be seen in cumulative summations where the salt water profiles take longer than the fresh water to reach an equivalent fraction. These differences are fairly small and the profiles converge with increased forcing.

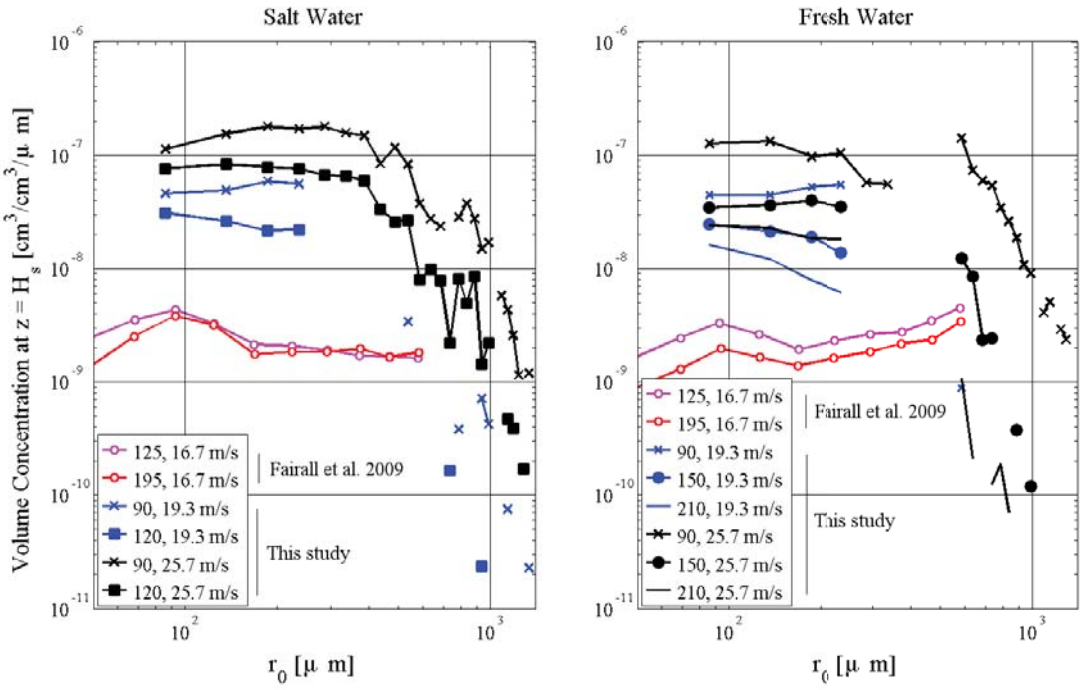

Figure 5. Size-dependent spray volume concentrations transformed to the theoretical source level ($z = H_s$) for salt (left) and fresh (right) water, as in the volume of spray per unit volume of air per radius increment. The legend entries denote the height above the MWL of the original observation point in mm and the wind forcing in m/s. Note that these wind speeds are in a lab reference frame, as opposed to the 10-m winds referenced throughout this work. This is done to make fair comparisons to Fairall *et al.* [24] (magenta and red curves in both panels), who did not report scaled wind speeds. 25.7 m/s and 19.3 m/s correspond to the 54 m/s and 40.5 m/s wind speed trials reported within this study, respectively.

The number concentrations from equation (1) can be converted to volume concentrations by multiplying by $4/3\pi r_i^3$ and transforming down to the theoretical source height, H_s, using methods described in Fairall *et al.* [24] (figure 5). It is expected that for a given wind speed and radius class the volume concentrations observed at various heights above this level should all collapse to the "source" value. A convergence within 0.5 orders of magnitude is observed, which is slightly more than reported by Fairall *et al.* [24], but is nonetheless fairly consistent with accepted theories. It should be noted that the Fairall *et al.* [24] study used 24 ppt water to simulate oceanic salinities, which differs from the present work that utilized filtered sea water (32–34 ppt) for the saline trials. Also, the spectra from that study were smoothed to fill in gaps while the curves from the observations presented here were not.

With regards to the ASIST data, fresh and salt water spectra are remarkably similar. This does not agree with observations reported by Fairall *et al.* [24], where fresh and salt water show markedly different behavior for particles >200 µm (see figure 5). In that work these differences were attributed largely to evaporation as well as a potential sampling bias. The wind forcing dependence across water salinities is markedly similar, which is in agreement with previous observations [24]. These findings provide indirect confirmation that bubble production is not an important spume generation mechanism, because bubbles are known to be larger in fresh water versus salt water.

5. Future work

This study has attempted to characterize the vertical distribution of spume particles observed above breaking waves in both fresh and salt water states in a series of laboratory experiments. To first order salinity seems to play little role in the production of spume particles in high winds; however, differences in both the vertical profiles and particle radius spectrum were noted. Further investigation into the affect that this has on the vertical spray flux will be the focus of future efforts.

Acknowledgments

This work is supported by the NSF through grant 0933943. The authors appreciate the efforts of Mike Rebozo and Neil Williams for their help with the data collection. Professor M. Donelan is thanked for the acquisition of and permission to use previously collected data in ASIST.

References

[1] Fairall C, Kepert J and Holland G 1994 *Glob. Atmos. Ocean Syst.* **2** 121–142
[2] Donelan M A, Haus B K, Reul N, Plant W J, Stiassnie M, Graber H C, Brown O B and Saltzman E S 2004 *Geophys. Res. Lett.* **31** 5
[3] Powell M D, Vickery P J and Reinhold T A 2003 *Nature* **422** 279–83 ISSN 0028-0836
[4] Potter H, Graber H C, Williams N J, Collins C O, Ramos R J and Drennan W M 2015 *J. Atmos. Sci.* **72** 104–118 ISSN 0022-4928
[5] Pielke R A and Lee T J 1991 *Boundary-Layer Meteorol.* **55** 305–308 ISSN 0006-8314 URL `http://link.springer.com/10.1007/BF00122582`
[6] Soloviev A V, Lukas R, Donelan M A, Haus B K and Ginis I 2014 *Sci Rep* **4** 5306 URL `http://www.ncbi.nlm.nih.gov/pubmed/24930493`
[7] Lewis E R and Schwartz S E 2004 *Sea Salt Aerosol Production: Mechanisms, Methods, Measurements, and Models - A Critical Review* (American Geophysical Union) ISBN 0875904173
[8] Jones K F and Andreas E L 2012 *Q. J. R. Meteorol. Soc.* **138** 131–144 ISSN 00359009
[9] Soloviev A and Lukas R 2010 *Boundary-Layer Meteorol.* **136** 365–376 ISSN 00068314
[10] Anguelova M, Barber R P and Wu J 1999 *J. Phys. Oceanogr.* **29** 1156–1165 ISSN 0022-3670
[11] Andreas E L 2004 *J. Phys. Oceanogr.* **34** 1429–1440 ISSN 0022-3670
[12] Barenblatt G I, Chorin A J and Prostokishin V M 2005 *Proc. Natl. Acad. Sci. U. S. A.* **102** 11148–11150 ISSN 0027-8424
[13] Bye J a T and Jenkins A D 2006 *J. Geophys. Res.* **111** 1–9 ISSN 0148-0227
[14] Andreas E L 1992 *J. Geophys. Res.* **99** 14345 ISSN 0148-0227
[15] Andreas E L and Emanuel K a 2001 *J. Atmos. Sci.* **58** 3741–3751 ISSN 0022-4928
[16] Andreas E L 2005 *Atmos. Res.* **75** 323–345 ISSN 01698095
[17] Andreas E L, Jones K F and Fairall C W 2010 *J. Geophys. Res. Ocean.* **115** 1–16 ISSN 21699291
[18] Jeong D, Haus B K and Donelan M A 2012 *J. Atmos. Sci.* **69** 2733–2748 ISSN 0022-4928
[19] Melville W K 1996 *Annu. Rev. Fluid Mech.* **28** 279–321
[20] Haus B K, Jeong D, Donelan M A, Zhang J A and Savelyev I 2010 *Geophys. Res. Lett.* **37** n/a–n/a ISSN 00948276
[21] Christensen M and Thomassen P 2014 *Experimental Determination of Bubble Size Distribution in a Water Column by Interferometric Particle Imaging and Telecentric Direct Image Method* Masters thesis Aalborg University
[22] Asher W and Farley P 1995 *J. Geophys. Res.* **100** 7045–7056
[23] Saffman M 1987 *Appl. Opt.* **26**
[24] Fairall C W, Banner M L, Peirson W L, Asher W and Morison R P 2009 *J. Geophys. Res.* **114** C10001 ISSN 0148-0227 URL `http://doi.wiley.com/10.1029/2008JC004918`